THE JOURNAL OF PHYSICAL CHEMISTRY B

ARTICLE

pubs.acs.org/JPCB

Regulation of Electron and Proton Transfer by the Protein Matrix of Cytochrome *c* Oxidase

Vangelis Daskalakis,[†,¶] Stavros C. Farantos,[†,‡] Victor Guallar,[§] and Constantinos Varotsis[*,⊥]

[†]Institute of Electronic Structure and Laser, Foundation for Research and Technology—Hellas, P.O. Box 1527, 711 10 Heraklion, Greece

[‡]Department of Chemistry, University of Crete, P.O. Box 2208, 710 03 Heraklion, Greece

[§]Life Sciences Department, Barcelona Supercomputing Center (BSC), 080 34 Barcelona, Spain

[⊥]Department of Environmental Management, Cyprus University of Technology, P.O. Box 50329, 3603 Lemesos, Cyprus

ABSTRACT: Cytochrome *c* oxidase (CcO) catalyzes the four-electron reduction of molecular oxygen to water and couples this reduction to the pumping of four protons through the protein matrix. Water molecules inside the protein are involved in the proton pumping activity as proton carriers. A highly conserved water molecule, among different CcO enzymes, lies between the heme a_3 propionates. Here, we show, by quantum mechanical/molecular mechanical (QM/MM) simulations, that this conserved water molecule can transfer its proton to propionate-A. His403 residue coordinates to the Mg site near the so-called *water pool*. By both QM/MM and molecular dynamics calculations, we demonstrate that the also conserved His403 residue, adjacent to the heme a_3 propionate-A, plays a role of a valve controlling the protonation state of the propionate-A/Asp399 pair. This, in turn, controls the oxidation state of the heme a_3 iron, linking in this way, the D-proton pathway to the water pool.

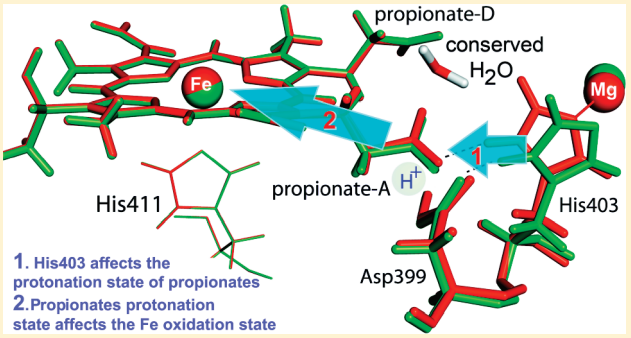

I. INTRODUCTION

Cytochrome *c* oxidase (CcO) couples the one-electron oxidation of cytochrome *c* to the four-electron reduction of molecular oxygen. These electron transfers are linked to proton translocation across the inner mitochondrial membrane or the bacterial cytoplasmic membrane. The enzyme contains four redox centers; two hemes *a* and three associated copper atoms. Electron injection from cytochrome *c* to the homodinuclear copper center, Cu_A, is followed by intramolecular electron transfer, via the low-spin heme *a*, to the binuclear center which contains a high-spin heme a_3 and a Cu_B atom. The latter two species serve as the catalytic site where O_2 is reduced to H_2O. The heme a_3/Cu_B active site complex is shown in Figure 1A.[1] The free energy released in the electron-transfer reactions is conserved as an electrochemical proton gradient across the inner mitochondrial membrane and is used ultimately for the synthesis of ATP. In this paper, we will use the residue numbering of aa_3 from *P. denitrificans*, where applicable and if not otherwise stated.

Bacterial and mammalian CcOs exhibit two relatively well-defined proton intake pathways, named D and K.[2] A discrete water exit pathway has been identified that involves water ligation to the Mg metal which is located near the heme a_3/Cu_B binuclear active center (Figure 1A).[3] The latter pathway was resolved by monitoring the magnetic interaction of ^{17}O-labeled water molecules, produced by the reduction of $^{17}O_2$ in CcO, with the Mg (Mn) metal, after 8 ms of the reaction start. Water molecules could act as proton carriers transferring protons during enzymatic turnover, and several research groups have suggested important structural as well as functional roles of specific amino acids and these water molecules near the active site.[3−9] The presence of water molecules in a hydrophobic cavity near the Glu278 of D-pathway connecting it to the heme a_3 propionate-D (prop-D) and Cu_B has been proposed based also on theoretical calculations.[5,6,10−12] In this line, the presence of water molecules in this hydrophobic cavity has been implicated in a mechanism in which Glu278 acts like a proton shuttle and/or as a valve.[4,13] In addition, a reversible redox-state-dependent dissociation of the prop-D/arginine salt bridge has been proposed to be triggered by the hydration of the heme a_3 ring D propionate, via the proposed D-pathway.[14]

As CcO function requires the coordinated transfer of protons and electrons, water molecules as well as protons are unlikely to randomly diffuse inside the enzyme. Such diffusion could compromise its proton-pumping functionality, easing the thermodynamically favorable back-leaking of protons which would short circuit the enzymatic pump.[14] In view of this, there should exist several control mechanisms/points for proton trapping in and around the active site with amino acids acting as proton valves. As previously stated, the Glu278 amino acid acts like such a valve at the entrance of the D-pathway of CcO. This residue controls the flow of protons from the mitochondrial matrix site to the

Received: December 6, 2010
Published: March 16, 2011

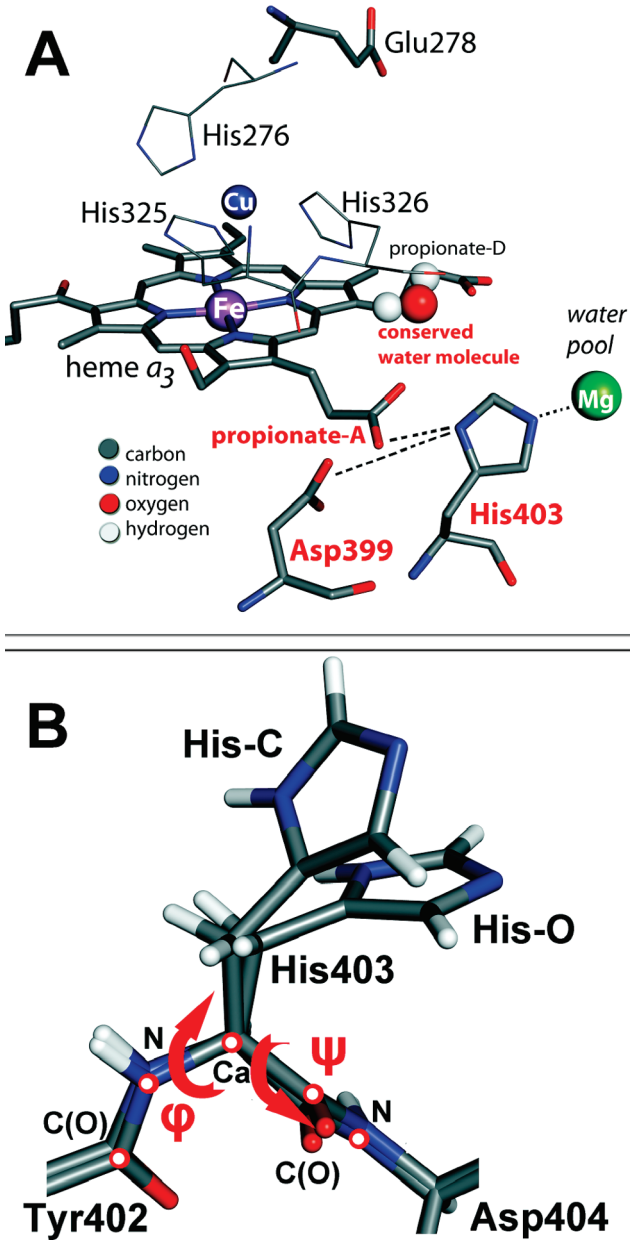

Figure 1. (A) Active site of aa_3 cytochrome *c* oxidase from *P. denitrificans*. His403 is able to exist in two different conformations: open (His-O), forming a His403···propionate-A strong hydrogen bond, or closed (His-C), forming a His403···Asp399 strong hydrogen bond. (B) Possible conformational change of His403 and the effect on the φ and ψ backbone peptide bond angles.

intermembrane space. While Glu278 orientation is dependent on the heme a_3/Cu_B oxidation states,[13] it also enables or halts proton motion, through the D-pathway, based on its protonation state.[4]

The characterization of the functional/structural implications of conserved residues in CcO in controlling proton and electron transfer to the distinct exit water channel, and the determination of the factors controlling the oxidation of heme a_3 during the O_2 reduction, will lead to a better understanding of the oxidative phase of CcO.

In this work, we probe theoretically the properties of the propionate-A (prop-A)/Asp399 and His403 triad along with the conserved H_2O molecule between the propionates. On the basis of our calculations, we propose that His403 is involved in controlling the protonation/deprotonation events of the heme a_3 propionate-H_2O-Asp399 in conjunction with the dynamics of the ligation of the exit Mg−H_2O pool. We show that His403 acts as a valve facilitating or halting the transfer of protons from the active site to the exit H_2O channel. Moreover, by controlling the protonation state of the heme a_3 prop-A/Asp399 pair, His403 affects, in turn, the oxidation state of heme a_3.

II. COMPUTATIONAL METHODS

All simulations were carried out with initial Cartesian coordinates from the crystal structure of a two-subunit aa_3 CcO from *Paracoccus denitrificans* (Protein Data Bank code 1AR1).[15a] Because of its smaller size, this two-subunit CcO protein from *P. denitrificans* serves as an analogue to the aa_3 oxidase from beef heart which has been extensively studied experimentally. Subunits I and II show a high degree of homology between these two enzymes coming from different organisms.[15a] Protonation states of amino acids like histidine, aspartic, and glutamic were checked visually and corrected when needed to reproduce hydrogen-bonding networks or electrostatic interactions with metals like Cu, Fe, Mg, and Ca. A Tyr280-His276 *cross-link* was added. Residue Glu278, acting as a proton shuttle or valve, at the entrance of D-proton pathway was set protonated. Histidine residues 403, 411, and 325−326 were set protonated at N_δ sites, while His276 was set deprotonated at both N_ε and N_δ sites to coordinate Cu_B and be cross-linked to Tyr280. The rest of the titratable sites were also checked and compared against the results from the H++ online protonation state prediction algorithm of Virginia Tech at pH 7.[16]

We treat models of oxy ($Fe^{II(III)}$−$O_2^{(-)}$|Cu_B^{I}), ferryl (Fe^{IV}=O|Cu_B^{II}−OH), and hydroxyl (Fe^{III}−OH|Cu_B^{II}−OH) intermediates of the CcO + O_2 reaction. Crystallographic waters inside the protein structure were retained, and an additional box of at least 14 Å distance between protein and its boundaries, full of water molecules, was implemented. For all the solvent molecules the TIP3P force field (FF)[17] was used. Starting Cartesian coordinates were altered accordingly to fit the above oxidation states by adding oxygens (−O−O−, =O) or hydroxyls (−OH) coordinated to heme a_3 iron or the Cu_B metal when applicable. For each protein system, an initial minimization/relaxation process was performed by Desmond Software of Schrodinger Suite 2009, before each QM/MM calculation, and it was based on the default protocol proposed in the Desmond manual (D.E. Shaw Research).[18] The RESPA integrator implemented in Desmond was used to integrate the equations of motion. The minimization/relaxation protocol includes two stages of minimization (restrained and unrestrained solvent or protein) and four stages of short MD runs with gradually diminishing restraints and increasing the temperature with a time step of 2.0 fs.

A. QM/MM Methodology. For the QM/MM geometries, after the minimization/relaxation, we reduced the water buffer significantly by excluding every solvent molecule beyond a distance of 8 Å off the protein matrix and froze those waters beyond a 20 Å layer around heme a_3 iron to their minimized position. A cutoff distance of 100 Å was also set. All the QM/MM calculations were performed with the QSite module of Schrodinger Suite 2009.[18] The H-cap approach was used for the covalent QM-MM boundary region. For the calculations, heme

Table 1. Mulliken Spin Populations on the Different CcO + O_2 Reaction Intermediates Based on the QM/MM Calculations with the His403 Residue at the Open (His-O) or Closed (His-C) Conformation[a]

	oxy-2	oxy-3	ferryl	hydroxyl
His-O (open)	Fe(0.06)−O(0.47)−O(0.47)−Cu_B(0.02)	Fe(0.97)−O(0.35)−O(0.52)−Cu_B(0.13)	Fe(1.30)=O(0.76)/Cu_B(−0.52)−OH(−0.31)	Fe(1.01)−OH(0.06)/Cu_B(0.53)−OH(0.32)
His-C (closed)	Fe(0.06)−O(0.47)−O(0.47)−Cu_B(0.02)	Fe(1.03)−O(0.36)−O(0.52)−Cu_B(0.09)	Fe(1.30)=**O**(0.76)/Cu_B(−0.52)−OH(−0.30)	Fe(1.01)−OH(0.07)/Cu_B(0.53)−OH(0.32)

[a] Oxy-2 and oxy-3 intermediates represent structures with Fe II or Fe III oxidation state, respectively.

a_3 with a truncated hydroxylethyl farnesyl side chain with only three carbon atoms included, Cu_B, His325−326, His276, Tyr280, Asp399, His403, and the proximal His411, unless otherwise stated, constitute the QM part (treated at the b3lyp/lacvp* level of theory), while the rest of the protein is treated with an empirical potential (OPLS2005 FF).[19,20] The lacvp* basis set are a combination of the 6-31G* basis set with the lanl2dz effective core basis set. Specifically, the atoms H to Ar are described with the 6-31G* basis set while heavier atoms are modeled using the lanl2dz basis set (Dunning/Huzinaga valence double-ζ,[21] Los Alamos ECP plus DZ on Na−La, Hf−Bi[22−24]).

B. MD Methodology. We used initial Cartesian coordinates from the previously optimized QM/MM intermediates and charges fitted to quantum mechanical electrostatic potential (ESP) maps. These structure were again solvated (H_2O), neutralized (adding ions) to the final volume of a box of at least 14 Å distance between protein and its boundaries and minimized/relaxed with the protocol mentioned above. Fe=O, Fe−O−O−, Fe−OH, His411−Fe, Cu_B−OH, and Cu_B−His bonds were introduced with harmonic parameters based on our previously developed force field.[25] Angles, dihedrals, van der Waals, and 1−4 pair interactions were also added, accordingly, to fit the OPLS2005 FF parametrization standards, yielding a simulation box of around 90 000 atoms, including solvent (described as TIP3P model).[17] Based on this simulation box, 25 ns runs were started in NVT ensemble at energy equivalent to 300 K, with a potential tapering between 14 and 16 Å, a time step of 0.5 fs, and constraining heavy atom−hydrogen covalent bonds with a tolerance of 10^{-8} Å (eight iterations). Coulombic electrostatic interactions were also taken into account. The RESPA integrator implemented in Desmond was used to integrate the equations of motion. For the protein backbone of α-carbon atoms, C_α, we calculated the rmsd value for every simulation in relation to the initial one. This gave an rmsd plot versus time with rmsd values of less than 1.6 Å for every MD simulation of 25 ns.

B3LYP functional as well as the OPLS2005 force field are both well tested in such systems, like CcO, in theoretical calculations and have been proven accurate enough to describe mechanisms of action or electron transfers for biological system models.[26,27]

III. RESULTS AND DISCUSSION

A. QM/MM Simulations. In the preliminary work for the protein preparation and equilibration process, we chose to apply the default minimization/relaxation protocol, discussed above. We decided to temper with the simulation times in the four stages of the short MD runs in this protocol. We chose either to use the default protocol times (+0 ns) for a first set or to introduce an increase in these times (+2−5 ns) for a second set of structures for the QM/MM optimization process. For the same oxidation and the fully protonated Asp399/prop-A pair, we observed a flexibility of the His403 residue. Based on these findings, the amino acid was optimized at the QM/MM level in the next step in two different conformations, either with a strong hydrogen-bonding interaction with prop-A (Figure 1B, open conformation, His-O) or with Asp399 (Figure 1B, closed conformation, His-C) for each and every intermediate. Thus, we produced QM/MM-optimized structures of the oxy-2 (Fe^{II}/Cu^{I}), oxy-3 (Fe^{III}/Cu^{I}), ferryl, and hydroxyl intermediates with His403 residue in these two different conformations. This conformational change, apart from the side-chain orientation

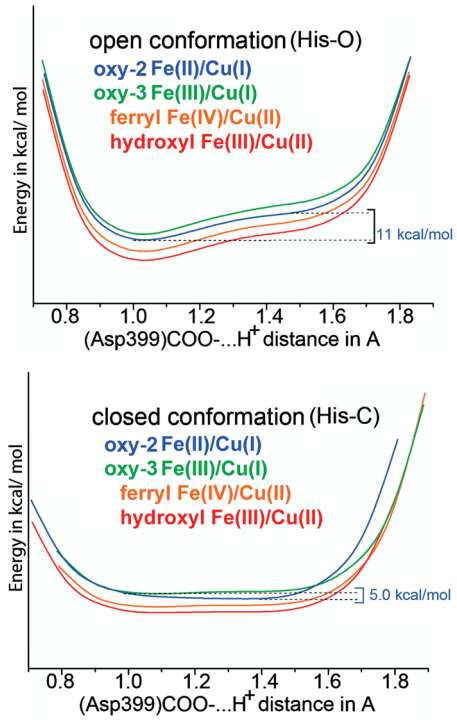

Figure 2. Diagrams derived from QM/MM calculations depicting the energy profiles of a proton (H^+) transfer from Asp399 to propionate-A in the open and closed conformations of His403 in the different heme a_3/Cu_B oxidation states.

change, introduces also backbone effects (Figure 1B). Specifically, for the ferryl intermediate, we observed changes in the φ = C(O)−N−C(a)−C(O) and ψ = N−C(a)−C(O)−N peptide dihedral bond angles (φ, ψ) from (−61.3, +121.1) for the His-O to (−58.3, +111.3) for the Hic-C conformation. The same trend was evident also in the other intermediates, concerning the His403 residue. Table 1 shows the spin population on the metal sites and coordinated oxygens (Mulliken analysis) for the open (His-O) and closed (His-C) His403 conformations. The two different oxy structures indicated in Table 1 represent different oxidation states of the heme a_3 iron (oxy-2 with Fe^{II} and oxy-3 with Fe^{III}).

Proton-transfer energy profiles were then generated for the multiple QM/MM optimized geometries of the several CcO + O_2 intermediate structures of either open or closed conformations of the His403 residue. These profiles were generated by increasing and freezing the Asp399···H^+ distance at steps of 0.1 Å in the Asp399···prop-A direction. For each step, we run single-point QM/MM calculations after a short equilibration step cycle with frozen Asp399···H^+ and prop-A···H^+ distances. The profiles in Figure 2 show that, in the open conformation, if only one proton is shared between Asp399 and prop-A, the H^+ is trapped on the Asp399 side, irrelevantly to the oxidation state of the active site. In the closed configuration and oxy-2 Fe(II)/Cu_B(I) state, the shared proton is trapped on the prop-A. The minima for a proton movement between prop-A and Asp399 become almost degenerate in the rest of the closed conformations. In these cases, His403 orientation facilitates the easy transfer of protons between the two carboxylic groups, like a closed circuit, hence the label "closed".

Taking the oxy-2 example (blue lines in Figure 2), it seems that the His-O to His-C transition introduces a change in the relative

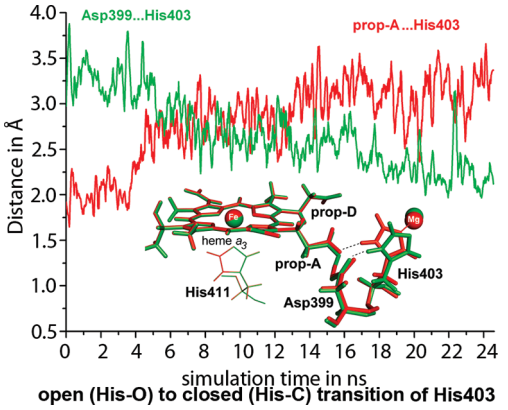

Figure 3. Molecular dynamics (MD) simulations depict the conformational change of His403 residue between two hydrogen-bonding states: open (red) and closed (green) in the ferryl, fully protonated propionate-A/Asp399 case (Desmond2009, NVT simulation, time step 0.5 fs, 300 K).

minimum protonation structures for the specific oxidation state of the active site. While for the His-O conformation the only shared proton between Asp399/prop-A resides on the Asp399 side (Asp399-H^+ is stabilized by −11 kcal/mol), it resides on the prop-A side when in the His-C conformation (prop-A-H^+ is stabilized by −5 kcal/mol). The two different isoelectronic His-O/His-C minima exert an absolute energy difference of around 69 kcal/mol, with the His-O being the lowest energy structure. For the rest of the oxidation states, the energy difference between His-O and His-C for the respective minima becomes around 72 kcal/mol for the oxy-3, 65 kcal/mol for the ferryl, and 63 kcal/mol for the hydroxyl. These large energy differences can be due to several factors like (a) the varying strength of the electrostatic interactions between (His403) N_δ-H···prop-A and (His403) N_δ-H···Asp399, with the protonation state of the carboxylic groups playing a key role; (b) the varying energy of the prop-A-H^+ and Asp399-H^+ species; (c) the steric hindrance introduced upon the His-O to His-C transition, exerted also as the φ and ψ dihedral peptide angles change, and (d) due to local or global changes in the MM part of the structures, as His-C and His-O systems have been independently relaxed/equilibrated with different simulation times in the four stages of short MD runs (see paragraph III of Computational Methods). This latter factor is difficult to control and evaluate in a large QM/MM system of around 28 000 atoms including the water solvent.

The potential energy curves in the cases of oxy-3, ferryl, and hydroxyl of the His-C conformation (Figure 2) exert flatness over a range of almost 0.8 Å (between ∼0.9 and 1.6 Å of the Asp399···H^+ distance). Over that range, the shared proton H^+ between Asp399 and prop-A is loosely interacting with both carboxylic groups and hence it can be easily transferred to other sites in the area, or even to water molecules. The instability of that proton, when His403 orientation is closed, could provide a key step in the mechanism of proton movement in the area or proton release out of the active site.

B. MD Runs. To test the extent and feasibility of the above His403 conformational changes, we performed MD simulations on the QM/MM optimized structures of the intermediates. MD simulations on solvated protein models of around 90 000 atoms, including solvent, indicated that His403 residue can interact with both prop-A and Asp399 changing between two conformations;

dx.doi.org/10.1021/jp1115993 |J. Phys. Chem. B 2011, 115, 3648–3655

either with a stronger prop-A/His403 (His-O) or a stronger Asp399/His403 (His-C) hydrogen bond. Such change is evident on the dynamics when both Asp399 and prop-A are protonated. This is due to the fact that protonated carboxyl groups of prop-A/Asp399 appear neutral and are free of strong electrostatic interactions with the H−N_δ proton of His403. This facilitates the observed flexibility of His403, in the area, to be shown on the MD trajectories.

The MD simulation trajectory on ferryl intermediate is shown in Figure 3 with the Asp399/prop-A pair fully protonated. The same trend and trajectories are observed on all the intermediates studied with both Asp399 and prop-A protonated. At an energy equivalent of 300 K the His403 residue is able to change from the His-O to the His-C conformation. We observed high transition energies for all intermediates at the QM/MM level, with the largest being at 72 kcal/mol (oxy-3), when only one proton is shared between Asp399 and prop-A (Figure 2). Based on the MD at 300 K results, it seems that this conformational change in energy, along with the assumed transition barrier, becomes low enough to enable such a transition in the case where both prop-A and Asp399 lose their negative charges by protonation. If the transition energies would remain large (63−72 kcal/mol), the MD trajectory of the ferryl intermediate of Figure 3 would not exert the His403 open to close transition at 300 K. Thus, the electrostatic interactions in the Asp399/prop-A/His403 triad are important and control the His-O to His-C transition. Neutralizing the charged interactions, by protonation, seems to be a crucial step in the process significantly lowering the His-O to His-C conformational barrier. In fact, calculating the QM/MM energy differences between His-O and His-C conformations of the several intermediates with both Asp399 and prop-A protonated, we observe a lowering of the gap by more than 20 kcal/mol compared to the cases where a single proton is shared between Asp399 and prop-A. The previously calculated energy differences of 63−72 kcal/mol of Figure 2 are lowered significantly at the same b3lyp/lacvp*, OPLS2005 level of theory. We have to note that we used different relaxation/minimization protocol for the His-O and His-C systems (see paragraph III of Computational Methods). Although we still calculate high energy differences between His-C and His-O conformations, even when both Asp399 and prop-A are protonated, we believe that these energy differences are mainly due to the minimization/relaxation protocol and setup of each His-O, His-C systems set in the first stages of the protein preparation process. Nevertheless, we cannot, in any case, overlook the lowering of these energy differences by more than 20 kcal/mol by the protonation of both Asp399 and prop-A.

Both geometry (QM/MM minimum energy) optimized structures and MD simulations contribute to the conclusion of a flexible His403 residue in the area of heme a_3 propionates. Compared to our previous work on the ferryl intermediate of ref 28, here we use a larger solvation box, inducing larger number of solvent molecules (water, TIP3P FF).

His403 residue plays a role, as a valve, controlling the flow of protons in the region. By substantially changing the pK_a values of the prop-A or Asp399, a proton is trapped or released by prop-A. His403 ligates the Mg site of the discrete water/proton exit pathway.[3] This adds to the significant role of His403 in the area of heme a_3 propionates. The orientation of the His403 could also be easily affected, transiently, by waters released from the active site on their way to the *water pool*. As the neutralization of the prop-A/Asp399 pair seems to be important for the process of the His-O to His-C transition, water molecules could easily undertake such a neutralization role.

C. Oxy $Fe^{II/III}-O_2/Cu^{I}$ Intermediate. The oxy intermediate appears to be more sensitive to the His403 orientation, as only in that case we observe a reverse on the minima for the different prop-A/Asp399 protonation states (Figure 2). In addition, we observed that the neutralization of the negative charges in the prop-A/Asp399 pair is important for the His-O to His-C conformational change to take place. In this consensus, we decided to further probe the protonation events in the area of the prop-A/Asp399/His403 triad focusing on the oxy oxidation level. We are interested also in protonating the prop-A/Asp399 pair on-the-fly during the QM/MM calculations. As mentioned in the Introduction, waters are possible sites for the accommodation of a H^+ in the form of transient hydronium (H_3O^+) species, acting as proton carriers.

Interestingly enough, as previously mentioned, a single water molecule is highly conserved in the crystal structures of bacterial and mammalian CcOs, between the heme a_3 propionates,[2,15] as seen in Figure 1A. This conserved water molecule, found in the crystal structures, lies between 2.2 and 2.8 Å from propionates A and D. In most crystal structures, as well as in that of aa_3 from *P. denitrificans* used herein, the conserved water is found closer to prop-D, but always in the area between propionate A and D of heme a_3.[15] Moreover, the prop-A/Asp399/His403 interactions are also conserved between the different CcO structures referenced in this study. This water lies within the proposed water exit hydrophilic pathway between the heme a_3 propionates and the water pool through the Mg site.[3] Being in close proximity to the propionates and, as a H_3O^+, being highly unstable in the environment of a protein,[12] it can easily provide its H^+ for the requested on-the-fly protonation events in the area.

For this reason, we increased the QM part of the QM/MM optimized oxy intermediate ($Fe^{II(III)}-O_2^{(-)}|Cu_B^{I}$) by adding such an H_3O^+. In the oxy model with protonated Asp399 and both heme a_3 propionates deprotonated, the H_3O^+ proton is transferred to the heme a_3 propionate-A on the QM/MM optimization process. This neutralizes the prop-A/Asp399 carboxylic charges. Although this water molecule moves during the initial minimization/relaxation protocol before the QM/MM simulations, it never escapes the boundaries of 2.2−2.8 Å distance to heme a_3 propionates A and D at the referenced simulation times. For consistency, we chose to include it in the QM part of the QM/MM calculations at the same place as in the crystal structure of *P. denitrificans*,[15a] adjusting manually its position after the minimization/relaxation protocol and before the QM/MM optimization, exactly as it appears in the original pdb file coded 1AR1. We believe that this assumption is consistent with the conserved presence of a water molecule in the crystal structures between the heme a_3 propionates.

In the course of each QM/MM optimization process, upon the proton transfer from the H_3O^+ to prop-A, the side chain of His403 changes conformation to form hydrogen bonds of almost equal strength to Asp399 and prop-A. In fact, equilibrated and optimized His403···prop-A and His403···Asp399 hydrogen-bonding distances of around 1.7 and 3.2 Å change to around 2.3 and 2.7 Å, respectively, upon the H^+ transfer to prop-A. This provides additional evidence of the flexibility and conformational transition of the His403 residue as well as its important role in the area near the active site. The prop-A/Asp399 pair has been proposed to take part in the proton pumping activity also previously.[25,29]

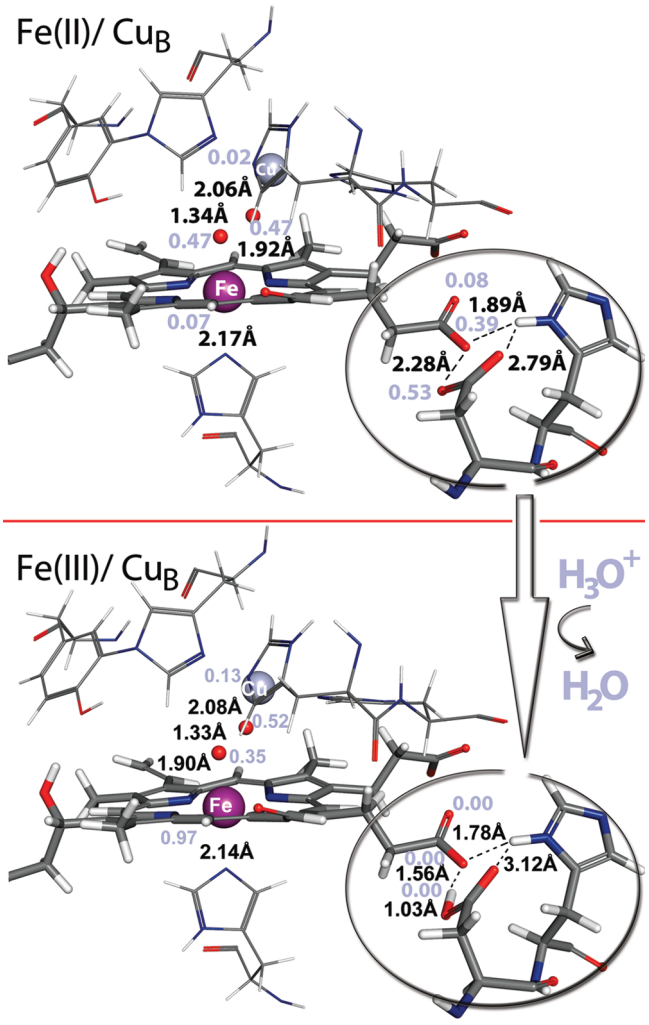

Figure 4. QM/MM-optimized isoelectronic geometries of the oxy intermediate with different oxidation states of heme a_3 iron II and III induced by the change in propionate-A/Asp399 protonation state. Interatomic distances like His−Fe, Fe−O, O−O, and O−Cu and H-bonding distances are depicted in black, while spin populations appear in light blue.

D. Spin Localization on Heme a_3 Propionate-A/Asp399 Pair. While we propose the role of the prop-A/Asp399 and His403 triad in regulating proton transfer near the Mg exit site, we should note that protonation events are coupled to the redox chemistry in CcO enzymes. By QM/MM probing of this triad in different protonation states (prop-A-/Asp399, prop-A-/Asp399-H^+) and heme a_3/Cu_B in the various oxidation states (oxy-2, oxy-3, ferryl, and hydroxyl), we observe that only in the oxy-2 Fe(II)/Cu_B(I) structure (multiplicity triplet) a localization of spin density is observed on the bicarboxylic prop-A/Asp399 fully deprotonated pair, both in open and closed His403 conformations. The orientation of this fully deprotonated prop-A/Asp399 pair in the oxy-2 optimized structure is consistent with the crystal structure,[15] while all other heme a_3/Cu_B oxidation states give distorted fully deprotonated prop-A-/Asp399 geometries due to the repulsion of negative charges in close proximity. Protons are available to this transient fully deprotonated prop-A/Asp399 pair through the D-pathway.[5,6,10−12] In the QM/MM calculation, by protonating this fully deprotonated prop-A/Asp399 pair, the structure is optimized to an isoelectronic protonated prop-A-/Asp399-H^+ species. This protonation also induces the oxidation of heme a_3 with Fe^{II} (spin population 0.07) to Fe^{III} (spin population 0.97) transition (Figure 4). The presence of both protonated and deprotonated forms of the ring A of heme a_3 propionate and the deprotonated form of Asp-372 (Cytochrome ba_3 from *Thermus thermophilus* numbering) has been determined by time-resolved Fourier transform infrared spectroscopy on the $ba_3(Fe^{II})$−CO complex.[29c] This provides an experimental evidence for the possibility of the existence of a fully deprotonated prop-A-/Asp399 or a prop-A-H^+/Asp399 pair, previously probed by the QM/MM calculations herein, in the case of aa_3 of *P. denitrificans* and the oxy-2 Fe^{II} intermediate.

The next step taken was to increase the QM area of the QM/MM calculations by adding the heme *a* redox center, adjacent to the heme a_3/Cu_B centers. The optimized structures are schematically shown in Figure 5 and compared to the ones with the smaller QM region of Figure 4. The highly CPU demanding and time-consuming QM/MM optimization process for both isoelectronic species, which include heme *a* on the QM site, introduces no significant differences compared to the spin populations calculated before with the smaller QM site. In fact, the only observable difference is a slight increase in the Cu_B spin population (from 0.13 to 0.25). Chances that the spin localization on prop-A/Asp399 pair could have been due to an artifact are lowered, as by including the adjacent redox center of heme *a* in the QM region of the QM/MM calculation the localization still stands. In favor of this is also the fact that this spin localization is not universally observable, but only in the oxy oxidation state.

Previous studies indicate that the propionate groups induce the delocalization of the spin density in the cytochrome P450cam putative active species, compound I,[30] but such a case has not yet been reported for CcO. In a recent study by Fee et al.,[31] the proton release driving force, in the active site region, is proposed to be an uncompensated positive charge (formally on Cu_B). This results in deprotonation of key residues, like the His ligands of Cu_B or the cross-linked Tyr residue also in Cu_B coordination sphere, during the enzymatic turnover. In contrast, our proposed mechanism of action and the driving force of proton/electron couplings are consistent with no deprotonation/protonation events on the Cu_B coordination sphere, in accordance with previous reports.[32,33] The spin localization identified on heme a_3 propionates, based on our study, consists of the underlying force inducing the required proton movement in the area of the active site. The important potential of prop-A/Asp399 pair to accommodate spin density and control the heme a_3 oxidation state in CcO enzymes, in accordance with the adjacent His403 acting as a pK_a regulator valve, must not be underestimated when studying CcO mechanisms of action. Thus, this study is in favor and in accordance to proposals of CcO mechanistic details which involve the prop-A/Asp399 pair.

E. Proton Transfer and Water Exit. During the enzymatic turnover, protonation states prop-A-H^+/Asp399- or prop-A-/Asp399-H^+ may accept a proton that in turn causes the release of a proton to the water pool.[29c,34] On the basis of our current QM/MM and MD study, we postulate that the His403 residue is involved in the controlling of the protonation states of the prop-A/Asp399 pair, enabling or halting the release of that proton out of the active site. The additional proton, coming from the D-pathway, neutralizes the prop-A/Asp399 charges and the His403 conformation changes to enable that release by

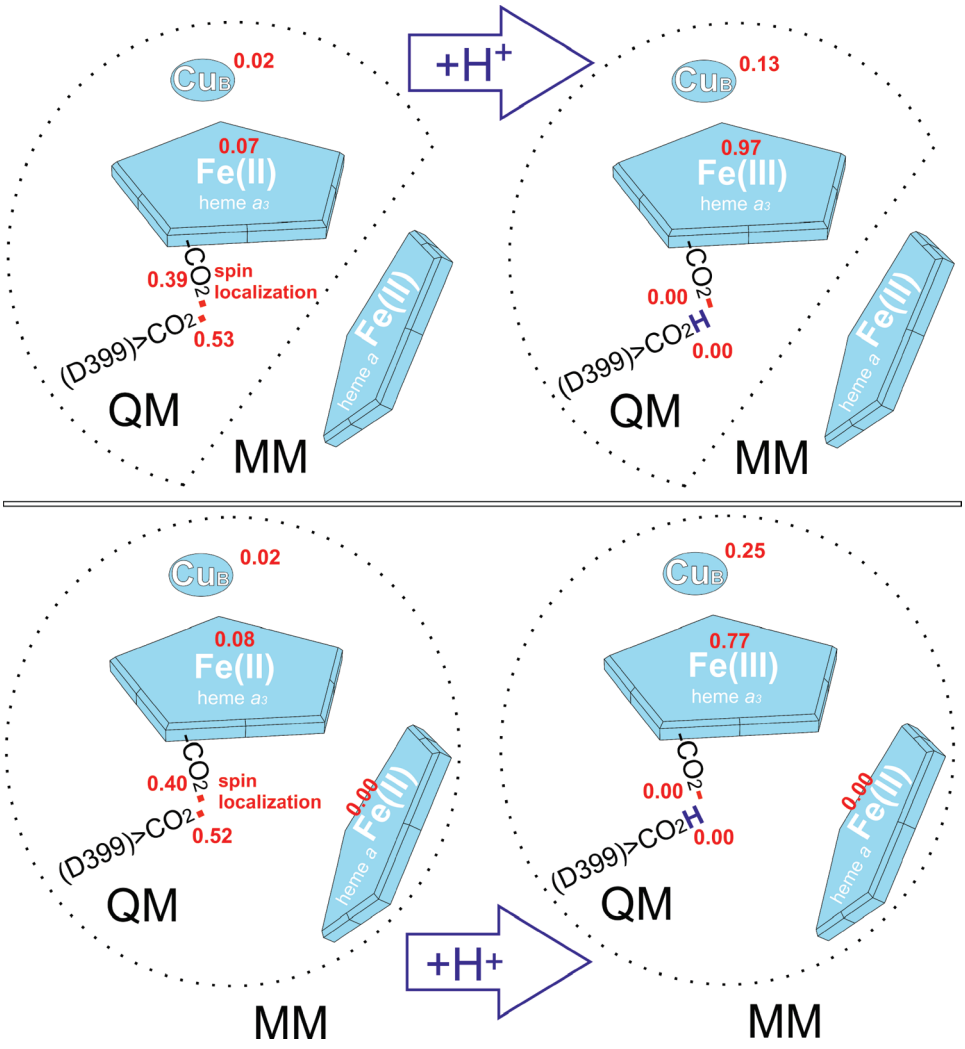

Figure 5. Schematic representation of QM/MM-optimized isoelectronic structures of the oxy intermediate with different oxidation states of heme a_3 iron II and III induced by the change in propionate-A/Asp399 protonation state. Two sets of structures are shown: with or without heme *a* metal site in the QM area. Spin populations appear in red.

converting a rather stable carboxylic proton (on Asp399 or prop-A) to a loosely interacting one. It seems that this proton release is also controlled by the oxidation state of the heme a_3/Cu_B active site, as it appears "blocked" in the case of the oxy-2 Fe^{II}/Cu_B^{I} intermediate.

The accumulation of H_2O molecules has been identified in the *P. denitrificans* oxidase, and their involvement in proton exit channels has been demonstrated by mutagenesis experiments.[29a,b] We consider that His403 orientation can be perturbed by the ligand water (H_2O) motion, as His403 is conveniently placed between the active site and the water pool. So, further investigation on the His403-Mg interaction would be of interest in future works.

IV. CONCLUSIONS

The results described herein define for the first time a direct link between the D-pathway and the water pool. Throughout this route there exist two proton valves and an electron/proton coupling site. Glu278 acts as the shuttle and the first valve for the release of a proton to Cu_B (chemical) and propionates (pumped).[4,13] Heme a_3 prop-A/Asp399 pair acts as the proton/electron coupling site. The His403 residue acts as the second valve for the trapping of a proton at the prop-A/Asp399 pair or its release out of the active site. The electrostatic interactions in the prop-A/Asp399/His403 triad are important in controlling the His403 conformational change, with the residue existing in two states with strong hydrogen bonding to either the heme a_3 ring A propionate or the Asp399. We demonstrate a facile proton pump pathway connecting the D-pathway to the water pool.

AUTHOR INFORMATION

Corresponding Author

*E-mail: c.varotsis@cut.ac.cy. Tel: +357 25002451. Fax: + 357 25002802.

Present Addresses

¶Department of Environmental Management, Cyprus University of Technology, P.O. Box 50329, 3603 Lemesos, Cyprus.

ACKNOWLEDGMENT

The work has been performed under the HPC-EUROPA2 project (no. 228398) with the support of the European Commission-Capacities Area-Research Infrastructures and the European

Union ToK grant GRID-COMPCHEM (MTKD-CT-2005-029583). V.D. is grateful to Prof. Guallar and to his research group for their hospitality and help, especially Dr. Fatima Lucas and Frank Wallrapp. This work is also supported by the Research Promotion Foundation (to C.V.).

REFERENCES

(1) (a) Ferguson-Miller, S.; Babcock, G. *Chem. Rev.* **1996**, *96*, 2889–2907. (b) Michel, H.; Behr, J.; Harrenga, A.; Kannt, A. *Rev. Biophys. Biomol. Struct.* **1998**, *27*, 329–356. (c) Belevich, I.; Verkhovsky, M. I. *Antioxid. Redox Signal* **2008**, *10*, 1–29. (d) Babcock, G. T.; Wikstrom, M. *Nature* **1992**, *356*, 301–309. (e) Wikstrom, M. K. F. *Nature* **1977**, *266*, 271–273.

(2) (a) Tsukihara, T.; Aoyama, H.; Yamashita, E.; Tomizaki, T.; Yamaguchi, H.; Shinzawa, N.; Nakashima, R.; Yaono, R.; Yoshikawa, S. *Science* **1995**, *269*, 1069–1074. (b) Fetter, J. R.; Qian, J.; Shapleigh, J.; Thomas, J. W.; Garcia-Horsman, A.; Schmidt, E.; Hosler, J.; Babcock, G. T.; Gennis, R. B.; Ferguson-Miller, S. *Proc. Natl. Acad. Sci. U.S.A.* **1995**, *92*, 1604–1608. (c) Iwata, S.; Ostermeier, C.; Ludwig, B.; Michel, H. *Nature* **1995**, *376*, 660–669. (d) Svensson-EK, M.; Abramson, J.; Larsson, G.; Tornroth, S.; Brezinski, P.; Iwata, S. *J. Mol. Biol.* **2002**, *321*, 329–339. (e) Tsukihara, T.; Shimokata, K.; Katayama, Y.; Shimada, H.; Muramoto, K.; Aoyama, H.; Mochizuki, M.; Shinzawa-Itoh, K.; Yamashita, E.; Yao, M.; Ishimura, Y.; Yoshikawa, S. *Proc. Natl. Acad. Sci. U.S.A.* **2003**, *100*, 15304–15309. (f) Muramoto, K.; Hirata, K.; Shinzawa-Itoh, K.; Yoko-o, S.; Yamashita, E.; Aoyama, H.; Tsukihara, T.; Yoshikawa, S. *Proc. Natl. Acad. Sci. USA* **2007**, *104*, 7881–7886. (g) Aoyama, H.; Muramoto, K.; Shinzawa-Itoh, K.; Hirata, K.; Yamashita, E.; Tsukihara, T.; Ogura, T.; Yoshikawa, S. *Proc. Natl. Acad. Sci. U.S.A.* **2009**, *106*, 2165–2169. (h) Koepke, J.; Olkhova, E.; Angerer, H.; Muller, H.; Peng, G.; Michel, H. *Biochim. Biophys. Acta* **2009**, *1787*, 635–645. (i) Muramoto, K.; Ohta, K.; Shinzawa-Itoh, K.; Kanda, K.; Taniguchi, M.; Nabekura, H.; Yamashita, E.; Tsukihara, T.; Yoshikawa, S. *Proc. Natl. Acad. Sci. U.S.A.* **2010**, *107*, 7740–7745.

(3) Schmidt, B.; McCracken, J.; Ferguson-Miller, S. *Proc. Natl. Acad. Sci. U.S.A.* **2003**, *100*, 15539–15542.

(4) Xu, J.; Voth, G. A. *Proc. Natl. Acad. Sci. U.S.A.* **2005**, *102*, 6795–6800.

(5) Riistama, S.; Hummer, G.; Puustinen, A.; Dyer, R. B.; Woodruff, W. H.; Wikström, M. *FEBS Lett.* **1997**, *414*, 275–280.

(6) Zheng, X.; Medvedev, D. M.; Swanson, J.; Stuchebrukhov, A. A. *Biochim. Biophys. Acta* **2003**, *1557*, 99–107.

(7) Voth, G. A. *Acc. Chem. Res.* **2006**, *39*, 143–150.

(8) Hofacker, I.; Schulten, K. *Proteins: Struct., Funct., Gen.* **1998**, *30*, 100–107.

(9) Wikstrom, M.; Verkhovsky, M. I.; Hummer, G. *Biochim. Biophys. Acta* **2003**, *1604*, 61–65.

(10) Puustinen, A.; Bailey, J. A.; Dyer, R. B.; Mecklenburg, S. L.; Wikstrom, M.; Woodruff, W. H. *Biochemistry* **1997**, *36*, 13195–13200.

(11) Tashiro, M.; Stuchebrukhov, A. A. *J. Phys. Chem. B* **2005**, *109*, 1015–1022.

(12) Olkhova, E.; Hutter, C.; Lill, M. A.; Helms, V.; Michel, H. *Biophys. J.* **2004**, *86*, 1873–1889.

(13) Kaila, V. R.; Verkhovsky, M. I.; Hummer, G.; Wikstrom, M. *Proc. Natl. Acad. Sci. U.S.A.* **2008**, *105*, 6255–6259.

(14) Wikstrom, M.; Ribacka, C.; Molin, M.; Laakkonen, L.; Verkhovsky, M.; Puustinen, A. *Proc. Natl. Acad. Sci. U.S.A.* **2005**, *102*, 10478–10481.

(15) (a) Ostermeier, C.; Harrenga, A.; Ermler, U.; Michel, H. *Proc. Natl. Acad. Sci. U.S.A.* **1997**, *94*, 10547–10553. (b) Tsukihara, T.; Aoyama, H.; Yamashita, E.; Takashi, T.; Yamaguichi, H.; Shinzawa-Itoh, K.; Nakashima, R.; Yaono, R.; Yoshikawa, S. *Science* **1996**, *272*, 1136–1144. (c) Yoshikawa, S.; Shinzawa-Itoh, K.; Tsukihara, T. *J. Bioenerg. Biomembr.* **1998**, *30*, 7–14.

(16) Gordon, J. C.; Myers, J. B.; Folta, T.; Shoja, V.; Heath, L. S.; Onufriev, A. *Nucleic Acids Res.* **2005**, *33*, Web server issue.

(17) Jorgensen, W. L.; Chandrasekhar, J.; Madura, J. D.; Impey, R. W.; Klein, M. L. *J. Chem. Phys.* **1983**, *79*, 926–935.

(18) http://www.schrodinger.com.

(19) Jorgensen, W. L.; Maxwell, D. S.; Tirado-Rives, J. *J. Am. Chem. Soc.* **1996**, *118*, 11225–11236.

(20) Jorgensen, W. L.; Tirado-Rives, J. *J. Am. Chem. Soc.* **1988**, *110*, 1657–1666.

(21) Dunning Jr., H. T.; Hay, P. J. *Modern Theoretical Chemistry*; Plenum: New York, 1976; Vol. 3.

(22) Hay, P. J.; Wadt, W. R. *J. Chem. Phys.* **1985**, *82*, 270–283.

(23) Wadt, W. R.; Hay, P. J. *J. Chem. Phys.* **1985**, *82*, 284–298.

(24) Hay, P. J.; Wadt, W. R. *J. Chem. Phys.* **1985**, *82*, 299–310.

(25) Daskalakis, V.; Farantos, S. C.; Varotsis, C. *J. Am. Chem. Soc.* **2008**, *130*, 12385–12393.

(26) Blomberg, R.A. M.; Siegbahn, E.M., P. *Biochim. Biophys. Acta* **2010**, *1797*, 129–142.

(27) Wallrapp, F.; Masone, D.; Guallar, V. *J. Phys. Chem. A* **2008**, *112*, 12989–12994.

(28) Daskalakis, V.; Farantos, S. C.; Guallar, V.; Varotsis, C. *J. Phys. Chem. B* **2010**, *114*, 1136–1143.

(29) (a) Kannt, A.; Lancaster, C. R.; Michel, H. *Biophys. J.* **1998**, *74*, 708–721. (b) Ostermeier, C.; Iwata, S.; Michel, H. *Curr. Opin. Struct. Biol.* **1996**, *6*, 460–466. (c) Koutsoupakis, C.; Soulimane, T.; Varotsis, C. *Biophys. J.* **2004**, *86*, 2438–2444.

(30) Guallar, V.; Baik, M.-H.; Lippard, S. J.; Friesner, R. A. *Proc. Natl. Acad. Sci. U.S.A.* **2003**, *100*, 6998–7002.

(31) Fee, A. J.; Case, A. D.; Noodleman, L. *J. Am. Chem. Soc.* **2008**, *130*, 15002–15021.

(32) Pinakoulaki, E.; Pfitzner, U.; Ludwig, B.; Varotsis, C. *J. Biol. Chem.* **2002**, *277*, 13563–13568.

(33) Daskalakis, V.; Pinakoulaki, E.; Stavrakis, S.; Varotsis, C. *J. Phys. Chem. B* **2007**, *111*, 10502–10509.

(34) Verkhovsky, M. I.; Jasaitis, A.; Verkhovskaya, M. L.; Morgan, J. E.; Wikstrom, M. *Nature* **1999**, *400*, 480–483.